Influence of Microstructures on Thermal Shock and Sintering Behavior of YSZ-based Thermal Barrier Coatings

Kirsten Bobzin, Lidong Zhao, Mehmet Öte, Tim Königstein

(Surface Engineering Institute, RWTH Aachen University, Kackertstr. 15, 52072 Aachen, Germany)

ABSTRACT: In this study, two thermal barrier coatings based on YSZ were produced by using a commercially available agglomerated and sintered powder and a special spray powder prepared by high energy ball milling. Both thermal barrier coatings exhibited similar overall porosities, but significantly different microstructures. Application of the special spray powder prepared by high energy ball milling led to a microstructure with numerous inclusions of semi-molten agglomerates, which introduced a plethora of clusters of fine pores into the coating and several more microstructural defects. This microstructure resulted in a significantly better thermal shock behavior compared to the conventional thermal barrier coating. The heat treatment of both thermal barrier coatings at θ=1150 ℃ for t=100 h led to a sintering of both coatings. The results were reduced overall porosity and significantly increased fracture toughness. A correlation between the fracture toughness of both coatings after the heat treatment and the thermal shock life time could not be identified.

KEY WORDS: thermal barrier coating; ZrO_2-7%Y_2O_3; high energy ball milling; thermal shock

中图分类号：TG174.4 **文献标识码：**A **文章编号：**1001-3660(2019)04-0028-06

DOI：10.16490/j.cnki.issn.1001-3660.2019.04.004

Introduction

Thermal barrier coatings (TBCs) are effective means to protect underlying metallic components in turbine engines from damages caused by excessive temperature and corrosion environments. TBCs consist typically of a ceramic top coat and a metallic bond coat. The top coat serves as a thermal barrier which delays the heat flow from the hot gas stream to the metal substrate, while the bond coat protects the substrate from oxidation and high temperature corrosion by forming of a thin and dense Al_2O_3-based scale at the ceramic/bond coat interface. Yttria partially stabilized zirconia ZrO_2-(7~8)wt%Y_2O_3 (YSZ) has been established as the standard material for the top coat in TBC systems in the last decades[1-5].

Because the properties of plasma-sprayed TBCs are influenced by their porous microstructures, the performance of TBCs can be improved by modifying their microstructure using special spray powders such as nanostructured powders[5-8]. Like nanostructured powders, the application of special spray powders prepared by high energy ball milling could significantly improve the performance of TBCs based on ZrO_2-4mol.% Y_2O_3-1mol.% Gd_2O_3-1mol.% Yb_2O_3[9, 10] as well, as a special porous microstructure with numerous inclusions of semi-molten agglomerates was formed. This microstructure resulted in a significantly lower thermal conductivity and a better thermal shock behavior compared to conventional TBCs. Semi-molten agglomerates could retain their clusters of pores after a long-term heat treatment at θ=1150 ℃ for t=500 h[10]. In this study, the effect of the special microstructure based on the spray powder prepared by high energy ball milling was investigated for a conventional YSZ system. A commercially available agglomerated and sintered YSZ spray powder was crushed by high energy ball milling. Subsequently, the crushed powder was agglomerated. TBCs were produced using both the agglomerated and sintered spray powder and the crushed and agglomerated spray powder. The spray parameters were chosen to allow both TBCs to exhibit similar overall porosities, which ensure a comparability of the influence of the pore structures. The influence of the microstructure on thermal shock and sintering behavior was investigated.

1 Experiments

In this study, a commercially available agglomerated and sintered ZrO_2-7 wt.%Y_2O_3 spray powder with

Received：2019-01-18；**Revised**：2019-02-10

Corresponding author: Lidong Zhao, E-mail: zhao@iot.rwth-aachen.de

a size distribution of d=−(90+16) μm (H. C. Starck GmbH, Goslar, Germany) was used as raw material for high energy ball milling and for the deposition of a reference TBC. The morphology of the powder was investigated by using the Zeiss LED 1530 (Carl Zeiss Microscopy GmbH, Germany) scanning electron microscope (SEM). The morphology is shown in Fig.1. The spray powder was crushed by the high energy ball mill Simoloyer CM08 (Zoz, Wenden, Germany). ZrO_2-3 wt.%Y_2O_3 ceramic balls (ϕ=5 mm and a total mass of m=5 kg) were applied as grinding media. The ball to powder mass ratio was r=10:1. The rotor turned with a rotation speed of n=1 000 r/min for t=4 min and subsequently with n=500 r/min for t=1 min in a cycle. The milling lasted t=60 min alltogether. The crushed powder was then agglomerated by using a binder (S Gel C1065W6, Wall Colmonoy Ltd, Swansea, Great Britain) with a mixing ratio of c=15 wt.%. After drying, the agglomerates were crushed and sieved to a powder size distribution of d=−(125+20) μm for spraying. Fig.2 shows the morphology of the crushed and agglomerated powder.

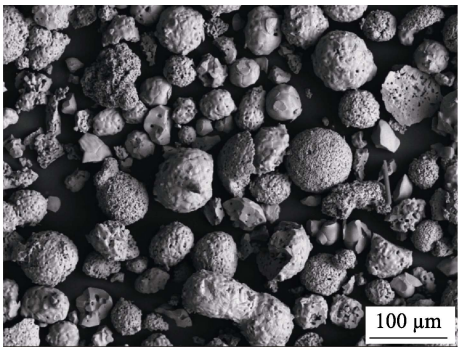

Fig.1 SEM micrograph of the agglomerated and sintered YSZ spray powder

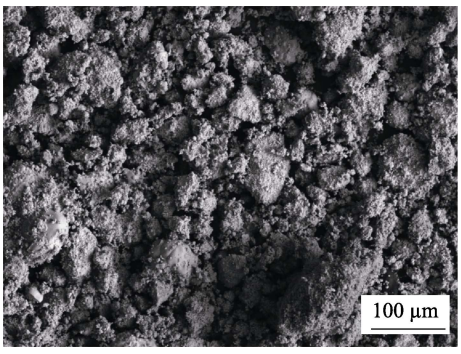

Fig.2 SEM micrograph of the crushed and agglomerated spray powder

The Ni-based super alloy Inconel 600 (ϕ 20× 5 mm) was used as substrate material. A NiCoCrAlY powder with a size distribution of d=−(63+22) μm was sprayed with a HVOF spray system DJ 2600 (Oerlikon Metco Europe GmbH, Kelsterbach, Germany) to form the bond coat. The parameters for DJ2600 are shown in Tab.1. A reference TBC deposited by using the agglomerated and sintered spray powder (in the following marked as TBC_R) and a TBC deposited by using the crushed and agglomerated powder (in the following marked as TBC_M) were produced by using a three-cathode plasma generator TriplexPro^{TM}-210 (Oerlikon Metco Europe GmbH, Kelsterbach, Germany). The parameters for the TriplexPro^{TM}-210 are shown in Tab.2. Based on the parameter development, the spray parameters were chosen to ensure that both TBCs exhibited similar overall porosities. In this way, the influence of the pore structures could be comparatively determined as the influence of the amount of the overall porosity was minimized. An X-ray diffraction analysis by using an XRD 3000 (Seifert, Hamburg, Germany) with a Cu target was carried out to determine the phase compositions of both TBCs. The microstructures were investigated by means of optical light microscopy and SEM. In addition to both TBCs, thick free-standing coatings (d=1.4~1.8 mm) were produced from both spray powders. The densities of the free-standing coatings in as-sprayed condition were ascertained by the water immersion method using Archimedes' Principle. The overall porosity in this study was defined as the ratio of the coating density to the density of a fully dense YSZ with a value of ρ=6.05 g/cm^3[11].

Tab.1 Parameters of the NiCoCrAlY bond coat by DJ2600 system

H_2 (SLPM)	O_2 (SLPM)	Shroud gas N_2 (SLPM)	Carrier gas N_2 (SLPM)	Stand off-distance/mm
666	214	300	40	270

Tab.2 Parameters of plasma spray with TriplexPro^{TM}-210

	YSZ powder fraction/μm	Current/A	Plasma gas Ar (SLPM)	Plasma gas N_2 (SLPM)	Distance/mm
TBC_R	−(90 +16)	450	60	8	210
TBC_M	−(125 +20)	450	66	—	80

Thermal cyclic tests were carried out in a furnace integrated into a test rig, similar to the ones described in [12]. The aim was to evaluate their thermal shock behavior. During the thermal cycles, samples were heated up to θ=1150 ℃ in the furnace, driven out of the furnace after a holding time of t=30 min and cooled down to θ=65 ℃ using compressed air. The cycles were repeated until the degradation of TBC reached approximately 20%. Degradation was measured by comparing the defect areas to the original area of the coatings. An isothermal heat treatment of the free-standing coatings was carried out in an electric furnace at θ=1150 ℃ for

t=100 h to investigate their sintering behavior. The fracture toughness of the free-standing coatings in as-sprayed condition and after the heat treatment were determined according to the equation $K_{IC}=0.015\cdot\left(\frac{E}{H}\right)^{\frac{1}{2}}\cdot\frac{P}{C^{\frac{3}{2}}}$ (E: Young′s modulus, H: hardness, P: load, C: crack length)[13,14]. The Vickers hardness testing under a load of F=4.9 N was done to generate indentations with microcracks. The Young′s modulus was estimated by using the measured indentation modulus of the coating. The indentation modulus was determined by means of an indentation tester Fischerscope HM 2000 (Helmut Fischer GmbH, Sindelfingen-Maichingen, Germany).

2　Results and Discussion

Fig.3 shows a light micrograph and an SEM micrograph of a cross-section of TBC_R in as-sprayed condition. A typical porous microstructure with differently-sized globular pores is well recognizable in the light micrograph. Apart from globular pores, intrasplat microcracks and intersplat porosities are well recognizable in the SEM micrograph. The measured density of TBC_R amounts to ρ=4.63 g/cm^3, leading to a calculated overall porosity of Φ=23%. Fig.4 presents a light micrograph and an SEM micrograph of a cross-section of TBC_M, showing a microstructure which is different from that of TBC_R. Apart from globular pores, intrasplat microcracks and intersplat porosities, numerous semi-molten agglomerates are included within TBC_M. As shown in the SEM micrograph, the semi-molten agglomerates introduced numerous clusters of fine pores into the coating. This microstructure presents the same characteristics as shown in [9, 10], indicating that the application of special spray powders prepared by high energy milling can reproducibly result in this kind of microstructure. This is suitable for different ceramic materials. The determined density of TBC_M amounts to ρ=4.73 g/cm^3, resulting in a calculated overall porosity of Φ=22%, which is only slightly lower than that of TBC_R.

Results of the thermal cyclic tests are presented in Fig.5. The average cycle numbers of TBC_R and TBC_M are 285 and 459 respectively. The average cycle number of TBC_M was more than 60% higher than that of TBC_R. The first failure for TBC_R occurred after 116 cycles, much earlier than that of TBC_M which was enhanced to more than 400 cycles. The interval between the maximal and the minimal cycle number among the four test samples for TBC_R was 306 cycles. In contrast, it was only 81 cycles for TBC_M, showing that the failure distribution range of TBC_M was significantly narrower, thus TBC_M was significantly more reliable than TBC_R. The results show that TBC_M had a significantly better thermal shock behavior than TBC_R. Because both TBCs exhibited similar overall porosities,

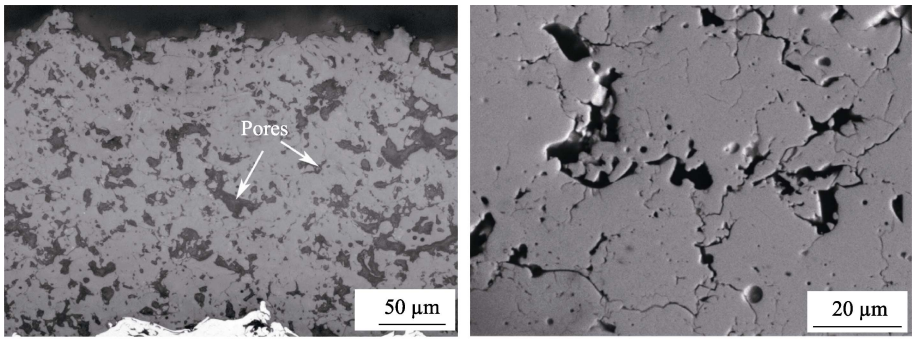

a Light micrograph　　b SEM micrograph

Fig.3 Micrographs of a cross-section of TBC_R

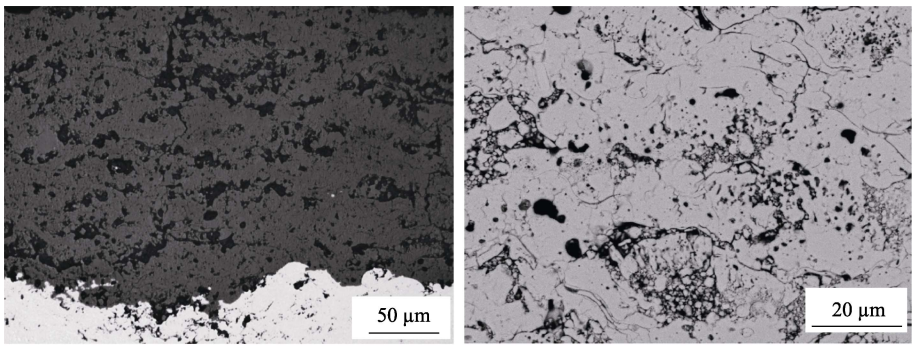

a Light micrograph　　b SEM micrograph

Fig.4 Micrographs of a cross-section of TBC_M

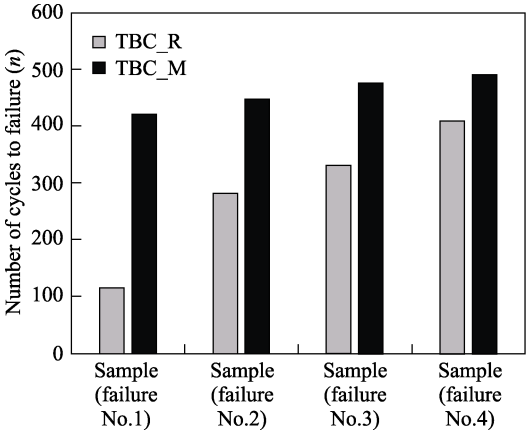

Fig.5 Results of the thermal cyclic test

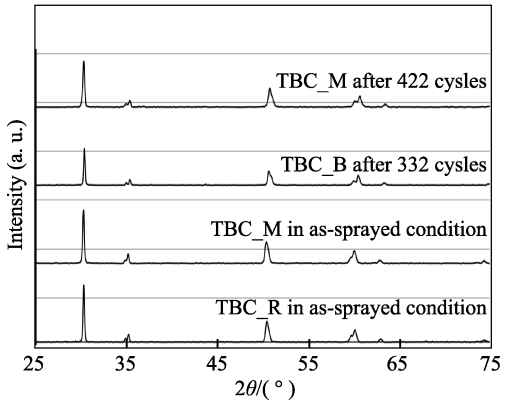

Fig.8 X-ray diffraction patterns of TBC_R and TBC_M in as-sprayed condition as well as after thermal cycle tests

the large deference in the thermal shock behavior was attributed to the different microstructures. Fig.6 and Fig.7 show light micrographs of cross-sections of TBC_R after 332 cycles and of TBC_M after 422 cycles. The cross-sections of the TBCs show that both TBCs fractured partly within the YSZ coat close to the interface with the TGO and partly through the TGO scale. A noticeable difference between both TBCs is that vertical microcracks formed in TBC_M. Such vertical microcracks could improve the thermal shock behavior, similar to segmented cracks in TBCs[15]. Fig.8 shows X-ray diffraction patterns of TBC_R and TBC_M in as-sprayed condition as well as after the thermal cyclic tests. No phase changes can be detected in the X-ray diffraction patterns. This confirms again that the microstructural difference was the main reason for their different thermal shock behavior.

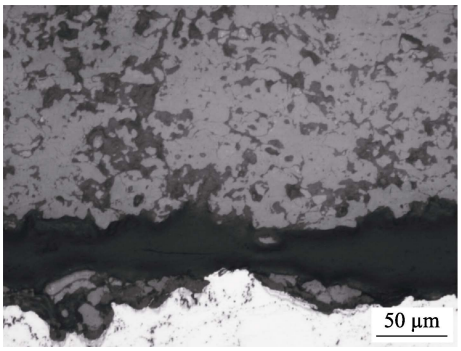

Fig.6 Light micrograph of a cross-section of TBC_R after 332 cycles

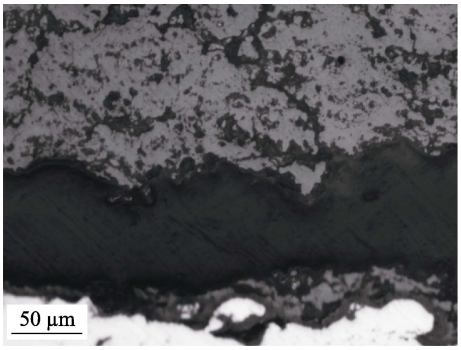

Fig.7 Light micrograph of a cross-section of TBC_R after 422 cycles

Thick, free-standing TBC_R and TBC_M were isothermally heat-treated in a furnace at θ=1150 ℃ for t=100 h. Fig.9 and Fig.10 show SEM micrographs of TBC_R and TBC_M after the heat treatment. Both TBCs remained porous. Big globular pores were barely affected by the heat treatment. However, the narrow microcracks as well as particle boundaries closed partly due to sintering, as marked in both SEM-micrographs. Semi-molten agglomerates are clearly recognizable, because they retained their cluster of pores despite sintering. The density of TBC_R increased to ρ= 4.80 g/cm^3 after the heat treatment. Based thereon, the calculated overall porosity amounts to Φ=21%. The density of TBC_M after t=100 h at θ=1150 ℃ had a value of ρ=4.88 g/cm^3. The calculated overall porosity amounts to Φ=19% correspondingly. The porosity of TBC_M decreased by 14%, which is higher than the 9% decrease for TBC_R. Due to the higher amounts of microstructural defects, sintering effect was more pronounced in case of TBC_M. The fracture toughness determined for free-standing TBC_R in as-sprayed condition amounts to $K_{IC}=1.89\ \mathrm{MPa}\cdot\mathrm{m}^{\frac{1}{2}}$. The fracture toughness significantly increased to $K_{IC}=2.39\ \mathrm{MPa}\cdot\mathrm{m}^{\frac{1}{2}}$ after t=100 h at θ=1150 ℃. The sintering improved the mechanical properties of TBC. The determined fracture toughness of TBC_M in as-sprayed condition amounts to $K_{IC}=1.26\ \mathrm{MPa}\cdot\mathrm{m}^{\frac{1}{2}}$. This value is significantly lower compared to TBC_R. This can be traced back to the amount of microstructural defects such as fine pores, microcracks and particle boundaries in the microstructure of TBC_M. The fracture toughness of TBC_M significantly increased to $K_{IC}=1.89\ \mathrm{MPa}\cdot\mathrm{m}^{\frac{1}{2}}$ after t=100 h at θ=1150 ℃. The increase amounts to 52%,

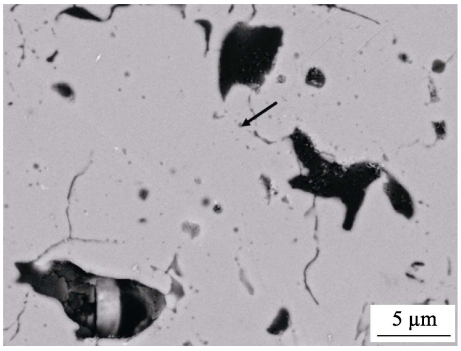

Fig.9 SEM micrograph of TBC_R after t=100 h at θ=1150 ℃

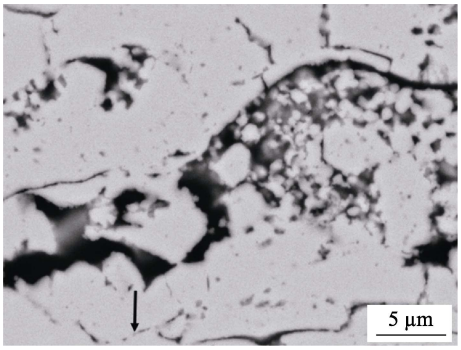

Fig.10 SEM micrograph of TBC_M after t=100 h at θ=1150 ℃

which is higher than that of TBC_R which exhibited an increase of 26%. This was again attributed to the higher amounts of microstructural defects in TBC_M. The results indicate that the form, size and distribution of microstructural defects in TBC influenced strongly sintering behavior for similar overall porosities. The fracture toughness of TBC_M after the heat treatment was still lower than that of TBC_R. But the difference is significantly smaller compared to the as-sprayed condition. It is noticeable that the fracture toughness of free-standing coatings cannot be correlated with the cycle numbers of both TBCs. Although the fracture toughness values of TBC_M are lower than those of TBC_R, TBC_M exhibited significantly better thermal shock behaviour. The reason could be that the microstructure of both TBCs changed differently during the cyclic tests than during the heat treatment.

3 Conclusions

In this study, two porous TBCs based on YSZ with similar overall porosities (Φ=23% and Φ=22%) were produced using a commercially available agglomerated and sintered powder and a special spray powder prepared by high energy ball milling. Both TBCs were investigated in terms of their microstructures, thermal shock performances and sintering behaviors. The results showed that both TBCs exhibited significantly different microstructures despite their similar overall porosities. The application of the special spray powder prepared by high energy ball milling led to a microstructure with numerous inclusions of semi-molten agglomerates, which introduced numerous clusters of fine pores into the coating and caused at the same time a higher number of microstructural defects like microcracks and boundaries. This special microstructure resulted in a significantly better thermal shock behavior compared to the conventional TBC. The heat treatment of both TBCs at θ=1150 ℃ showed that sintering occurred. The overall porosity decrease was significantly pronounced for TBC_M in comparison to TBC_R. The fracture toughness of both TBCs increased significantly due to sintering. A correlation between the fracture toughness after the heat treatment and the thermal shock behavior could not be identified. Generally, the results confirmed again that high energy ball milling is a suitable process for preparing spray powders to improve the TBC performance as it was already shown in previous studies[9, 10]. This method can be used for different ceramic materials.

Acknowledgements

The authors would like to thank the German Science Foundation (DFG) for financially supporting the research work within the scope of the DFG projects ZH205/2-1 and BO1979/32-2.

References

[1] PADTURE N P, GELL M, JORDAN E H. Thermal barrier coatings for gas-turbine engine applications[J]. Science, 2002, 296: 280-284.

[2] LI C J, LI Y, YANG G J, et al. A novel plasma-sprayed durable thermal barrier coating with a well-bonded YSZ interlayer between porous YSZ and bond coat[J]. Journal of thermal spray technology, 2012, 21: 383-390.

[3] ZHAO Y, WANG L, YANG J, et al. Thermal aging behavior of axial suspension plasma-sprayed yttria- stabilized zirconia (YSZ) thermal barrier coatings[J]. Journal of thermal spray technology, 2015, 24: 338-347.

[4] GAO L H, GUO H B, WEI L L, et al. Microstructure and mechanical properties of yttria stabilized zirconia coatings prepared by plasma spray physical vapor deposition[J]. Ceramic international, 2015, 41: 8305-8311.

[5] WU J, GUO H B, ZHOU L, et al. Microstructure and thermal properties of plasma sprayed thermal barrier coatings from nanostructured YSZ[J]. Journal of thermal spray technology, 2010, 19: 1186-1194.

[6] LIMA R S, MARPLE B R. Toward highly sintering-resistant nanostructured ZrO_2-7wt% Y_2O_3 coatings for TBC applications by employing differential sintering[J]. Journal of thermal spray technology, 2008, 17: 846-852.

[7] LIMA R S, MARPLE B R. Thermal spray coatings engineered from nanostructured ceramic agglomerated powders for structural, thermal barrier and biomedical applications: a review[J]. Journal of thermal spray technology, 2007, 16: 40-63.

[8] LIANG B, DING C. Thermal shock resistances of nanostructured and conventional zirconia coatings deposited by atmospheric plasma spraying[J]. Surface and coatings technology, 2005, 197: 185-192.

[9] BOBZIN K, ZHAO L, ÖTE M, et al. Deposition and characterization of thermal barrier coatings of ZrO_2-4 mol.% Y_2O_3-1 mol.% Gd_2O_3-1 mol.% Yb_2O_3[J]. Surface and coatings technology, 2015, 268: 205-208.

[10] BOBZIN K, ZHAO L, ÖTE M, et al. Effect of long-term heat treatment at 1150 ℃on the microstructure and properties of thermal barrier coatings based on ZrO_2-4 mol.% Y_2O_3-1 mol.% Gd_2O_3-1 mol.% Yb_2O_3[J]. Surface and coatings technology, 2017, 318: 142-146.

[11] LAN W H, XIAO P. Fabrication of yttria-stabilized-zirconia thick coatings via slurry process with pressure infiltration[J]. Journal of the european ceramic society, 2009, 29: 391-401.

[12] BOBZIN K, LUGSCHEIDER E, BAGCIVAN N. Thermal cycling behavior of lanthanum zirconate as EB-PVD thermal barrier coating[J]. Advanced engineering materials, 2006, 8: 653-657.

[13] QI H Y, YANG X G, WANG Y M. Interfacial fracture toughness of APS bond coat/substrate under high temperature[J]. International journal of fracture, 2009, 157: 71-80.

[14] WACHTMAN J B. Mechanical properties of ceramics[M]. New York: Wiley, 1996, 392.

[15] GUO H B, VASSEN R, STOVER D. Atmospheric plasma sprayed thick thermal barrier coatings with high segmentation crack density[J]. Surface and coatings technology, 2004, 186: 353-363.